Structural Basis of Binding of High-Affinity Ligands to Protein Kinase C: Prediction of the Binding Modes through a New Molecular Dynamics Method and Evaluation by Site-Directed Mutagenesis

Youngshang Pak,[†,‡] Istvan J. Enyedy,[†] Judith Varady,[†] Justin W. Kung,[§] Patricia S. Lorenzo,[§] Peter M. Blumberg,[§] and Shaomeng Wang*[,†]

Lombardi Cancer Center and Departments of Oncology and Neuroscience, The Research Building, Room WP05, Georgetown University Medical Center, Washington, D.C. 20007, and Laboratory of Cellular Carcinogenesis and Tumor Promotion, Division of Basic Sciences, National Cancer Institute, National Institutes of Health, Bethesda, Maryland 20892

Received November 16, 2000

The structural basis of protein kinase C (PKC) binding to several classes of high-affinity ligands has been investigated through complementary computational and experimental methods. Employing a recently developed *q*-jumping molecular dynamics (MD) simulation method, which allows us to consider the flexibility of both the ligands and the receptor in docking studies, we predicted the binding models of phorbol-13-acetate, phorbol-12,13-dibutyrate (PDBu), indolactam V (ILV), ingenol-3-benzoate, and thymeleatoxin to PKC. The "predicted" binding model for phorbol-13-acetate is virtually identical to the experimentally determined binding model for this ligand. The predicted binding model for PDBU is the same as that for phorbol-13-acetate in terms of the hydrogen-bonding network and hydrophobic contacts. The predicted binding model for ILV is the same as that obtained in a previous docking study using a Monte Carlo method and is consistent with the structure−activity relationships for this class of ligands. Together with the X-ray structure of phorbol-13-acetate in complex with PKCδ C1b, the predicted binding models of PDBu, ILV, ingenol-3-benzoate, and thymeleatoxin in complex with PKC showed that the binding of these ligands to PKC is governed by a combination of several highly specific and optimal hydrogen bonds and hydrophobic contacts. However, the hydrogen-bonding network for each class of ligand is somewhat different and the number of hydrogen bonds formed between PKC and these ligands has no correlation with their binding affinities. To provide a direct and quantitative assessment of the contributions of several conserved residues around the binding site to PKC−ligand binding, we have made 11 mutations and measured the binding affinities of the high-affinity PKC ligands to these mutants. The results obtained through site-directed mutagenic analysis support our predicted binding models for these ligands and provide new insights into PKC−ligand binding. Although all the ligands have high affinity for the wild-type PKCδ C1b, our site-directed mutagenic results showed that ILV is the ligand most sensitive to structural perturbations of the binding site while ingenol-3-benzoate is the least sensitive among the four classes of ligands examined here. Finally, we have employed conventional MD simulations to investigate the structural perturbations caused by each mutation to further examine the role played by each individual residue in PKC−ligand binding. MD simulations revealed that several mutations, including Pro11 → Gly, Leu21 → Gly, Leu24 → Gly, and Gln27 → Gly, cause a rather large conformational alteration to the PKC binding site and, in some cases, to the overall structure of the protein. The complete abolishment or the significant reduction in PKC−ligand binding observed for these mutants thus reflects the loss of certain direct contacts between the side chain of the mutated residue in PKC and ligands as well as the large conformational alteration to the binding site caused by the mutation.

Introduction

Protein kinase C (PKC) comprises a family of ubiquitous signal transducing molecules that play a central role in cell growth, differentiation, and apoptosis. [1−4] All the PKC isozymes discovered to date, with the exception of PKCζ and PKCλ, are activated under physiological conditions through the binding to the cofactors phospholipid and the two second messengers, Ca^{2+} and diacylglycerol (DAG) (Ca^{2+} is required only for the Ca^{2+}-dependent PKC isozymes).[1−5] PKC is the primary receptor for the powerful tumor-promoting agents phorbol esters, ingenol esters, mezerein, and thymeleatoxin and for teleocidins and their structurally simpler congener indolactam (ILV).[6,7] These PKC ligands serve as structural mimetics of DAG[6,7] and bind to the two cysteine-rich domains (C1a, C1b) in PKC with nanomolar binding affinity.[8,9] While many of these PKC ligands function as powerful tumor promoters, under appropri-

* To whom correspondence should be addressed. Phone: (202) 687-2028. Fax: (202) 687-0617. E-mail: wangs@giccs.georgetown.edu.
[†] Georgetown University Medical Center.
[‡] Present address: Department of Chemistry, Pusan National University, College of Natural Sciences, Kumjeong-ku, Pusan 609-735, Korea.
[§] National Institutes of Health.

10.1021/jm000488e CCC: $20.00
Published on Web 04/24/2001

ate conditions some PKC ligands also possess potent antitumor-promoting or anticancer activity. Thus, phorbol-12-myristate-13-acetate (PMA) and mezerein are now in clinical trials for the treatment of leukemia. Another highly potent PKC ligand, bryostatin, is in clinical trials for the treatment of breast, ovarian, and other forms of cancer. Before the structure of either C1a or C1b was solved, a number of three-dimensional (3D) pharmacophore models[12−18] were proposed in an attempt to provide a structural basis for ligand binding to PKC. Since these 3D pharmacophore models were derived solely from the ligand structures themselves and structure−activity relationships (SARs), the models were only partially successful in providing a structural basis for the binding of these structurally diverse ligands to PKC.

A 3D structure of the PKCδ C1b domain in complex with phorbol-13-acetate was determined by Zhang et al. using X-ray crystallography.[11] This structural information provided us with an opportunity to achieve a better understanding of the structural basis of the interaction between diverse PKC ligands and PKC and helped overcome some of the deficiencies in previous studies that were based solely on the structures of the ligands. Insight into the binding of the PKC pharmacophore to its ligands should facilitate the structure-based design of novel PKC ligands. Recently, through computational docking simulation and site-directed mutagenic analysis, we were able to achieve a fundamental understanding of the interactions between one class of potent PKC ligands, exemplified by the indolactam V (ILV) with PKC.[19] Good agreement was found between the computational analysis, site-directed mutagenic results and previous comprehensive structure−activity relationships (SARs) for this class of compounds. Our studies demonstrated that computational docking and site-directed mutagenic analysis together provide an effective approach to achieving insights into protein−ligand interactions. Encouraged by our success in the study of ILV, we have extended our computational and experimental analyses to several new classes of ligands, including ingenol-3-benzoate and thymeleatoxin. The major focus of the current study is to investigate the "pharmacophore" of PKC binding to different, structurally diverse classes of high-affinity PKC ligands.

In general, the active conformation of a ligand bound to its receptor is not known a priori. Furthermore, the receptor may need to adjust its binding-site conformation to accommodate different classes of ligands. For these reasons, it may be important and even necessary to include both ligand and receptor flexibility in a docking study to be able to obtain the "correct" binding mode. In our previous computational docking study of ILV binding to PKC, we employed a flexible docking program (MCDOCK), which allowed the inclusion of ligand flexibility in docking simulations.[19] Since inclusion of receptor flexibility dramatically increased the computational demand for docking calculations, we made an assumption that the binding site of PKC is rigid and interacts with ILV and the phorbol esters with the same conformation. However, from our molecular dynamic simulations, it was found that a number of hydrophobic residues around the binding site are flexible. To overcome this deficiency, in the present study we have employed a very recently developed molecular dynamics technique based on generalized statistical mechanics theory, termed the *q*-jumping MD method,[20,21] to tackle the flexible molecular docking problem by including both ligand and receptor flexibility. The prediction of the binding models of several classes of high-affinity ligands to PKC, the site-directed mutagenetic analysis of these ligands binding to both wild-type PKC and its mutants, and the investigation of structural perturbation caused by the mutations are the subjects of this paper.

Method and Materials

Computational Docking Method. The generalized statistical mechanics was first formulated by Tsallis,[22,23] and later, Andricioaei and Straub[24,25] applied the concept to optimization of small peptide and atomic cluster simulations.

The main idea of the current MD scheme is to employ the generalized effective potential introduced by Andricioaei and Straub:[24,25]

$$\bar{U}_q(\mathbf{r}^N) = \frac{q}{\beta(q-1)} \ln[1 - (1-q)\beta(U(\mathbf{r}^N) + \epsilon)] \qquad (1)$$

where $\beta = 1/(k_B T)$ and ϵ is an arbitrary energy shift parameter to make the transformed energy term $U(\mathbf{r}^N)$ positive definite. As was shown previously,[20,21] $\bar{U}_q$ tends to exhibit a more delocalized and smoother pattern as q increases from 1.0 to a value larger than 1.0. In the limit of $q = 1.0$, $U(\mathbf{r}^N)$ is recovered. In a similar way to previous studies,[20,21] $\bar{U}_q$ in eq 1 was constructed by considering only the nonbonding interaction terms (i.e., van der Waals and electrostatic interactions). In the present MD run, with a certain probability P_j, the q value jumps from 1.0 to greater than 1.0 for a brief period τ, followed by a gradual relaxation of q back to 1.0 for another period τ'. This jumping procedure results in a modified equation of motion with scaled nonbonding interaction forces such that

$$m_i \frac{\mathrm{d}^2\mathbf{r}_i}{\mathrm{d}t^2} = -\nabla_{\mathrm{r}_i} U_{\mathrm{b}}(\mathbf{r}^N) - \alpha_q(\beta,\mathbf{r}^N)\cdot\nabla r_i U_{\mathrm{nb}}(\mathbf{r}^N) \qquad (2)$$

where $U_{\mathrm{b}}(\mathbf{r}^N)$ and $U_{\mathrm{nb}}(\mathbf{r}^N)$ are the bonding and the nonbonding energy terms, respectively, and $\alpha_q(\beta,\mathbf{r}^N)$ is a scaling function defined as

$$\alpha_q(\beta,\mathbf{r}^N) = 1; \quad q = 1.0$$

$$= \frac{q}{1 - (1-q)\beta(U_{\mathrm{nb}}(\mathbf{r}^N) + \epsilon)}; \quad q > 1.0 \qquad (3)$$

As was already discussed previously,[25] in barrier regions where the potential energy is large, $\alpha_q(\beta,\mathbf{r}^N)$ reduces the magnitude of the forces and thereby facilitates barrier crossing. Although canonical distributions cannot be obtained by the current scheme, because of the nonphysical jumping procedure, a possible algorithm leading to correct distributions was proposed.[20] The transformation in eqs 1 and 2 was implemented in the CHARMM program,[26] and the detailed *q*-jumping procedure was carried out by a CHARMM script. The CHARMM24 empirical force field[27] was used to describe the receptor (PKC), and all the necessary parameters for each ligand were generated by using the QUANTA program.[28] For energy evaluations, a distance-dependent dielectric model was employed with the nonbonding interactions truncated at 8 Å.

A total of four classes of PKC ligands were selected in this study, including two phorbol esters, phorbol-13-acetate (**1**) and phorbol-12,13-dibutyrate (PDBu, **2**), indolactam (ILV, **3**), ingenol-3-benzoate (**4**), and thymeleatoxin (**5**).

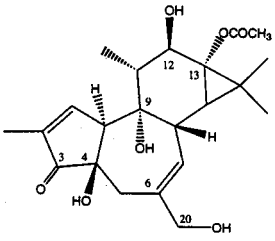

Phorbol-13-acetate (**1**)

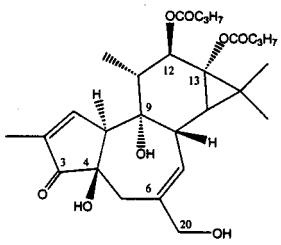

Phorbol-12, 13-dibutyrate (PDBu, **2**)

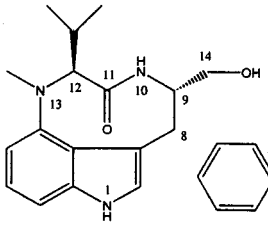

Indolactam (ILV, **3**)

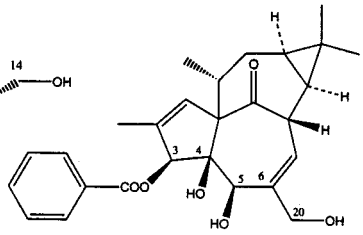

Ingenol-3-benzoate (**4**))

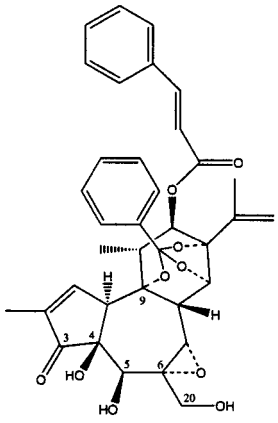

Thymeleatoxin (**5**)

The X-ray crystal coordinates were employed to describe the initial structure of phorbol-13-acetate.[11] It is known that indolactam (ILV) can exist in two conformations in solution (i.e., *cis*-twist and *trans*-sofa forms), and previous studies indicated that ILV most likely interacts with PKC in its *cis*-twist conformation.[19,29,30] Therefore only the *cis*-twist conformation was included in this investigation and the same coordinates used in the previous molecular modeling work were introduced for the initial structure of ILV. Starting from the phorbol-13-acetate structure in the X-ray crystal data, the initial conformations of both PDBu and thymeleatoxin were generated by QUANTA. For ingenol-3-benzoate, the crystal structure of the ingenol-3-tetradecanoate was used to provide the initial coordinates, but in this case the long hydrocarbon chain (tetradecanoate group) at position 3 was shortened by keeping only the first two for simplicity. This simplification can be justified because the hydrocarbon chain is not directly involved in the binding to PKC and is mainly responsible for binding to lipid membranes. All the appropriate hydrogen atoms were added to each ligand and minimized. Regardless of ligand type, the initial conformation of the receptor was obtained from the X-ray crystal structure of PKC C1b in complex with phorbol-13-acetate.[11] In this paper, the PKC residues corresponding to 231−281 are renumbered as 1−50. Then, by use of QUANTA, several initial conditions for the MD docking simulations were selected by placing each ligand in various orientations outside the PKC binding site. The ligands were allowed to be fully flexible, and all the side chains of the PKC residues 8−12 and 20−27 were allowed to be flexible; everything else in the receptor was fixed in our docking simulations. Then the MD simulations described above were carried out in a vacuum, using the following parameters: $q = 1.02-1.03$, $\epsilon = 800$, and $P_J = 0.1$.

The q-jumping MD simulations were carried out at $T = 300$ K, using the constant temperature algorithm of Berendesen,[31] and the SHAKE algorithm[32] was used to fix all the bonds containing hydrogen with a time step of 1 fs. Finally, NOE constraints consisting of a central atom of the ligand and each α-carbon atom in the PKC residues 10 and 24 were introduced to prevent the ligand from escaping from the binding site completely. With the MD protocol, we performed several independent MD runs for 1−2 ns, and the binding mode was determined from the lowest minimum energy conformation from each of the MD trajectories. Then the resulting complex structures were further refined by a minimization consisting of 5000 steps of the adopted Newton−Raphson method.

Analysis by Site-Directed Mutagenesis. (a) Plasmid Constructs and Site-Directed Mutagenesis. The cDNA encoding the second cysteine-rich domain of PKCδ (C1b domain) was subcloned into the GST prokaryotic gene fusion vector pGEX-2TK as described previously.[33] Point mutations in the C1b domain were generated by using the Unique Site Elimination (U.S.E.) Mutagenesis Kit (Pharmacia Biotechnology, Piscataway, NJ). The sequences of the primers employed were as described,[33] and all mutations were confirmed by sequencing (Paragon, Baltimore, MD). The different plasmids for the mutated C1b domains were used to express the corresponding GST-fusion proteins in *E. coli*.

(b) Ligand Binding Assay. The binding affinities of the isolated C1b domains of PKCδ were measured with [^{3}H]PDBu using the poly(ethylene glycol) precipitation method.[6] Briefly, purified GST-fusion proteins or total lysates from *E. coli* expressing the GST-fusion proteins (mutants and wild type) were incubated at 18 °C for 5 min in an assay mixture containing 100 μg/μL phosphatidylserine, 1 mM EGTA, [^{3}H]-PDBu, and, when appropriate, different concentrations of nonradioactive ligand such as PDBu or (−)-ILV. Proteins were precipitated by addition of 35% poly(ethylene glycol), and after centrifugation, the radioactivity in the supernatant and the pellet was assessed. Because [^{3}H]PDBu and ligands were found for the various constructs to reequilibrate rapidly, final ligand concentrations were used in all calculations.

Conventional Molecular Dynamics Simulation of PKCδ C1b and Its Mutants. The X-ray structure of PKCδ C1b in complex with phorbol-13-acetate was used as the starting structure for MD simulation of the wild-type PKC and for construction of the starting structures for all mutants. All Gly mutants were generated by replacing the side chain of the mutated residues with a hydrogen atom in the X-ray structure. All other mutants were generated by replacing the original side chain with a corresponding side chain in a similar orientation. The starting structure was solvated by inserting into a cubic TIP3P water box of 55 Å in each dimension. Water molecules whose oxygen atoms were less than 2.45 Å from any protein heavy atom were deleted.

All simulations were performed with the CHARMM program[26] using the all-atom parameter set from the CHARMM24 force field,[27] a constant dielectric $\epsilon = 1$, constant temperature $T = 300$ K, and constant pressure $p = 1$ atm. Temperature and pressure were kept constant using the Berendsen method.[31] Long-range electrostatic forces were treated with the force switch method in a switching range of 8−12 Å. van der Waals forces were calculated with the shift method and a cutoff of 12 Å. The nonbond list was kept to 14 Å. All bonds were constrained using the SHAKE algorithm.[32] The leapfrog method with a 2 fs time step was applied for numerical integration. Periodic boundary conditions were used with image update every 0.2 ps for water molecules. The distances between the Zn atoms and their coordinated S or N protein atoms in the protein were kept between 2 and 2.5 Å using NOE restraints. Each solvated protein was energy-minimized using 1000 cycles of steepest descent and 1000 cycles of adopted-basis Newton Raphson methods. This was followed by a 1.2−2.2 ns MD simulation for each mutant.

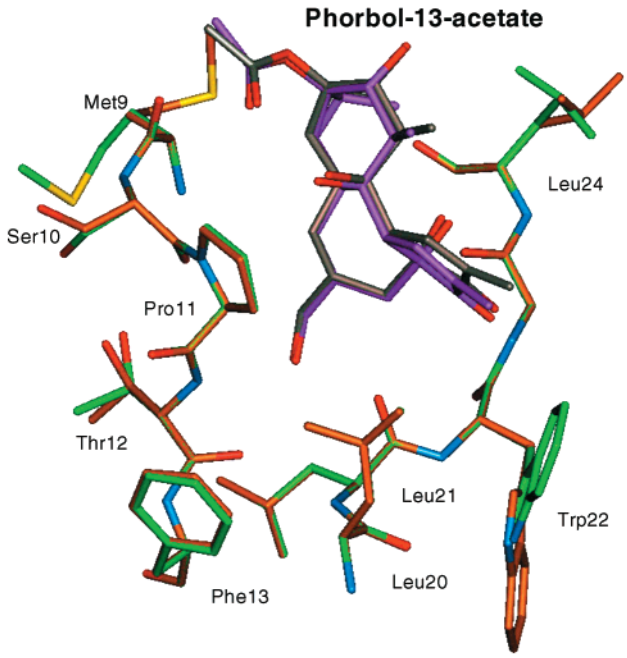

Figure 1. Superposition of the predicted binding model of phorbol-13-acetate (**1**) in complex with PKCδ C1b and the binding model determined by X-ray crystallography.

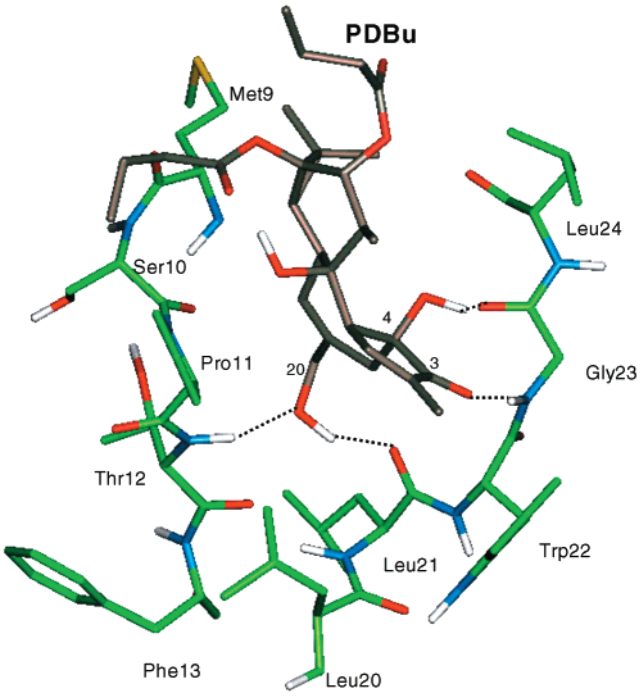

Figure 2. Predicted binding model of phorbol-12,13-dibutyrates (PDBu, **2**) in complex with PKCδ C1b. Hydrogen bonds are shown as dashed lines.

Results and Discussion

Prediction of the Binding Modes of PKC Ligands. The binding mode of PKC with phorbol-13-acetate determined from X-ray crystallography[10] was quickly located by the current simulations for 2 ns and was reproduced in several independent runs. The predicted binding mode was directly compared to the X-ray crystal structure. The root-mean-square deviation (rmsd) values of the predicted ligand and receptor positions are 0.2 and 0.9 Å, respectively, showing an excellent agreement with the X-ray determined binding mode. It is of interest to note that the somewhat large rmsd value of the receptor is mainly due to dynamic fluctuation of the side chains and that the most noticeable deviation occurs in Trp 22. The calculated binding mode superimposed with the crystallographic position is shown in Figure 1.

For the X-ray crystallographic study of PKC in complex with its ligands, it was necessary to select a PKC ligand with good aqueous solubility. For this reason, phorbol-13-acetate was selected despite its weak affinity. Phorbol-13-acetate has a K_i value of 13.8 μM, approximately 40000-fold less potent than phorbol-12,-13-dibutyrate (PDBu). The structures of phorbol-13-acetate and PDBu differ only in their hydrophobic side chains at positions 12 and 13; these side chains have been thought to be involved mainly in the interactions between the ligands and the membrane, a component in the usual assays for PKC binding to its ligands and PKC activation. It was thus assumed that these hydrophobic side chains on the ligands do not alter the binding mode of ligands to PKC, but this assumption had never been tested. We have therefore carried out studies on the docking of PDBu to PKC to investigate its binding mode and to compare it to that of phorbol-13-acetate.

By use of the same simulation procedure done for phorbol-13-acetate, the binding mode of PDBu to PKC was predicted (Figure 2) with several independent runs started with different initial configurations. The average rms value for PDBu between these predicted binding modes from independent runs was relatively small, less than 1 Å, suggesting that a unique binding mode was predicted, which was confirmed by graphic visualization. Comparison between the predicted binding for PDBu and the experimentally determined binding mode for phorbol-13-acetate showed that they are essentially the same; i.e., they have the identical hydrogen-bonding network and the same hydrophobic contacts between PKC and these two ligands. As was expected, the additional hydrophobic groups at positions 12 and 13 do not significantly increase the hydrophobic interactions between PKC and PDBu but are exposed to solvent. It has been suggested that binding of a PKC ligand to the C1a or C1b domain of PKC essentially changes the region around the ligand to hydrophobic, thus promoting effective interaction between the PKC−ligand complex and the membrane. The additional hydrophobic groups at positions 12 and 13 in PDBu should enhance the interactions between the PKC−ligand complex and the membrane. Furthermore, these additional hydrophobic groups increase the hydrophobicity of PDBu compared to phorbol-13-acetate and shift its equilibrium between membrane and aqueous phases. Since PDBu and phorbol-13-acetate have binding modes essentially identical to that of PKC and have similar hydrophobic contacts with PKC, the 40000-fold difference in their binding affinities should be mainly attributed to these two factors: the enhancement in the interactions between the PKC−PDBu complex and the membrane, and a more favorable partition for PDBu between membrane and aqueous phases.

Indolactam (ILV) represents a class of high-affinity PKC ligands with a ring structure different from other classes of PKC ligands. A number of simulations were

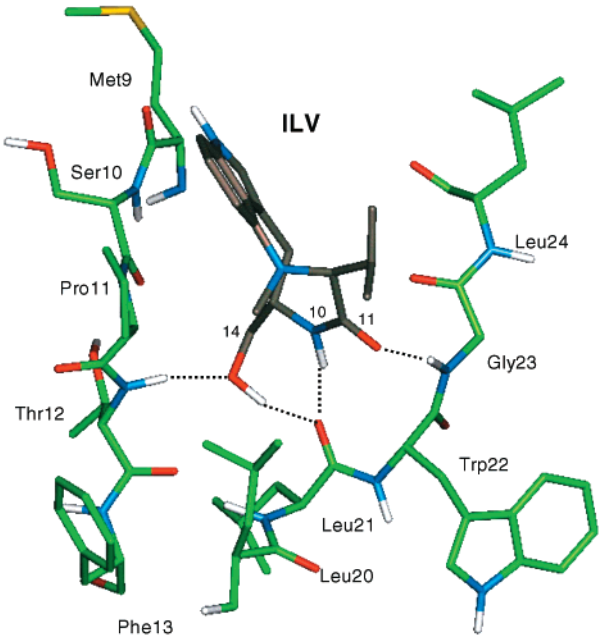

Figure 3. Predicted binding model of indolactam (ILV, **3**) in complex with PKCδ C1b. Hydrogen bonds are shown as dashed lines.

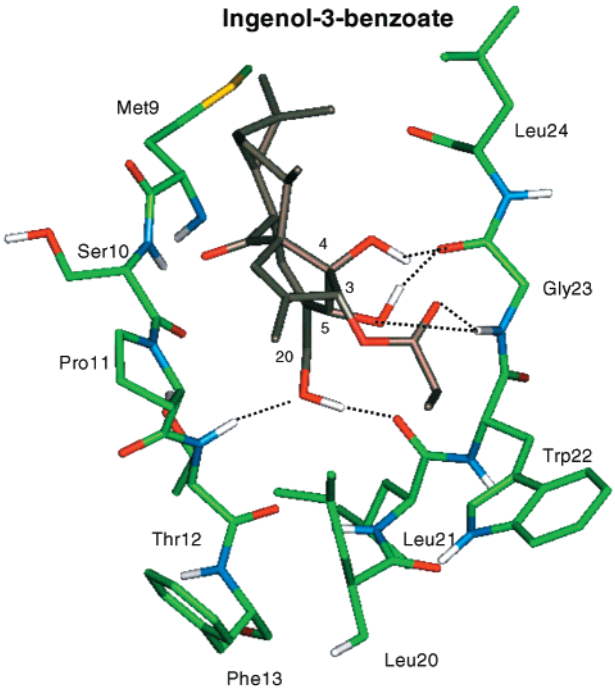

Figure 4. Predicted binding model of ingenol-3-benzoate (**4**) in complex with PKCδ C1b. Hydrogen bonds are shown as dashed lines.

performed starting with different configurations. A comparison between the binding models obtained with different starting configurations showed that a unique binding mode for ILV was predicted, as shown in Figure 3. As can be seen, the hydrogen-bonding network between ILV and PKC comprises four optimal hydrogen bonds. On the basis of the predicted and experimental binding modes for ILV and phorbol-13-acetate, it was found that these two classes of ligands shared three identical hydrogen bonds formed with the backbones of residues Thr12, Leu21, and Gly23 of the PKC. But each class of ligands has a unique hydrogen bond formed with PKC. For phorbol-13-acetate and PDBu, this unique hydrogen bond is formed between the hydroxyl group of the ligands at position 4 and the backbone carbonyl group of Gly23. For ILV, this unique hydrogen bond is formed between the amide group of the ligand at position 10 and the backbone carbonyl group of Leu21. In addition to these optimal hydrogen bonds, ILV also has a number of hydrophobic contacts between its hydrophobic groups and the hydrophobic side chains of PKC. For example, the *N*-methyl group of ILV is close to the hydrophobic side chain of Leu20 and Pro11, the isopropyl group at position 12 of ILV is close to the side chain of Leu24, and the indole ring of ILV resides on the top of the wall formed by Met9, Ser10, and Pro11 in PKC. The binding mode for ILV predicted using the current method is the same as that derived through Monte Carlo (MC) based computational simulations using the MCDOCK program and site-directed mutagenic analysis of crucial residues around the binding site.[19] It was found that the predicted binding mode of ILV was entirely consistent with structure−activity relationships (SARs) of ILV and the site-directed mutagenic data. Furthermore, on the basis of the predicted binding mode for ILV, we have successfully carried out a structure-based design of a novel class of PKC ligands.[39] Hence, the consistency between binding modes predicted by different simulation methods, the excellent agreement between the predicted binding model with experimental mutagenetic data and the SARs, and the successful structure-based design of a novel class of PKC ligands all support our predicted model for binding of ILV to PKC.

Ingenol-3-benzoate (**4**), with a K_i value of 0.13 nM, represents another class of high-affinity PKC ligands. Although its structure is also somewhat similar to that of PDBu, it has a number of structural elements including an ester group at position 3, an additional hydroxyl group at position 5, a carbonyl rather than a hydroxyl at position 9, and the lack of the ester groups at positions 12 and 13. A number of independent simulations starting with different initial configurations identified a binding mode with interaction energy substantially lower than those of other possible binding modes, as shown in Figure 4. Despite their different chemical structures, ingenol-3-benzoate and thymeleatoxin share the same hydrogen-bonding network. However, the ester carbonyl at position 3 of ingenol takes the place of the carbonyl group at position 3 in PDBu and phorbol-13-acetate as a hydrogen bond acceptor for the amide group of Gly23 of PKC.

Thymeleatoxin (**5**), which binds to PKC with a K_i value of 2.71 nM, represents another class of high-affinity PKC ligands. Although its basic structural skeleton is somewhat similar to the structures of phorbol esters, thymeleatoxin has a number of unique structural elements, including an additional hydroxyl group at position 5 and an epoxy group between positions 6 and 7. A number of independent simulations started with different configurations predicted a binding mode with interaction energy substantially lower than those of other binding modes, as shown in Figure 5. The hydrogen-bonding network between PKC and thymeleatoxin comprises a total of six optimal hydrogen bonds. All four hydrogen bonds formed between PKC and

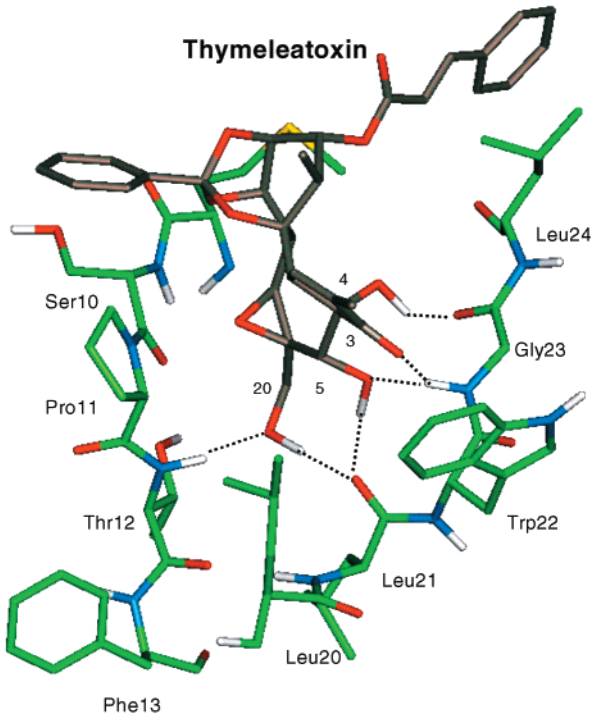

Figure 5. Predicted binding model of thymeleatoxin (**5**) in complex with PKCδ C1b. Hydrogen bonds are shown as dashed lines.

PDBu are found in the hydrogen bond network between PKC and thymeleatoxin. However, thymeleatoxin forms two additional hydrogen bonds between its hydroxyl group at position 5 and the amide group of Gly23 and the carbonyl group of Leu21 of PKC. Comparison between the hydrogen bond networks for ILV and thymeleatoxin showed that these two ligands also shared four common hydrogen bonds but thymeleatoxin has two additional hydrogen bonds formed between its hydroxyl group at position 4 and the carbonyl group of Gly23 of PKC and between its hydroxyl group at position 5 and the amide group of Gly23 of PKC. The hydrophobic contacts between thymeleatoxin and PKC closely mimic those between PDBu and PKC.

Previously, a number of pharmacophore models[12−18] were proposed on the basis of the analysis of the 3D structures of several classes of high-affinity PKC ligands. All these pharmacophore models were developed on the basis of the idea that these high-affinity PKC ligands share three or four common hydrogen bond donors and/or acceptors, which could be superimposed in a 3D space and could interact with common binding elements on PKC. In one such pharmacophore model, a common hydrophobic binding region was also included.[18] These pharmacophore models were partially successful in guiding PKC ligand design.[34,38]

Our present study provides new insights into the PKC pharmacophore. From our results, it is clear that a total of two hydrogen bond donors and two hydrogen bond acceptors, namely, the backbone amide groups of Thr12 and Gly23 and the backbone carbonyl groups of Leu21 and Gly23, participate in hydrogen-bonding interactions with PKC ligands. Although the two amide groups may form two optimal hydrogen bonds with PKC ligands, the two carbonyl groups may form up to four optimal hydrogen bonds because the carbonyl oxygen has two lone pairs of electrons. Thymeleatoxin and ingenol form all six of these possible hydrogen bonds, whereas phorbol-13-acetate, PDBu, and ILV form only four of these six possible hydrogen bonds. These four classes of PKC ligands only share one common hydroxyl group and one common carbonyl group, which form three common hydrogen bonds with the amide group of Thr12, the carbonyl group of Leu21, and the amide group of Gly23 of PKC, as shown in Figures 1−5. In addition to these three common hydrogen bonds, each PKC ligand has one or more additional hydrogen bonds with PKC. Phorbol-13-acetate and PDBu have an additional hydrogen bond formed between their hydroxyl group at position 4 and the carbonyl group of Gly23 of PKC. ILV has one additional strong hydrogen bond between its amide group at position 11 and the carbonyl group of Leu21 of PKC, and it has one weak hydrogen bond between its NH group at position 1 and the carbonyl group of Met9 of PKC. Thymeleatoxin has three additional hydrogen bonds formed between its hydroxyl group at position 4 and the carbonyl group of Gly23 of PKC and between its hydroxyl group at position 5 and both the carbonyl group and the amide group of Gly23 of PKC. Ingenol has three additional hydrogen bonds formed between its hydroxyl group at position 4 and the carbonyl group of Gly23 of PKC and between its hydroxyl group at position 5 and both the carbonyl group and the amide group of Gly23 of PKC. Three important conclusions may be drawn from this study: (1) These high-affinity PKC ligands indeed share three common hydrogen bonds, which may be defined as common pharmacophore elements, and these hydrogen bonds may be essential for the specificity of ligands binding to PKC. (2) Each class of PKC ligands has one or more additional hydrogen bonds formed with PKC that may not be shared by other classes of PKC ligands. (3) The number of hydrogen bonds formed between a ligand and PKC does not necessarily correlate with the binding affinity of a PKC ligand, but a ligand may need to form a number of hydrogen bonds for its specific binding to PKC.

From our study, it is also clear that the hydrophobic groups in these PKC ligands contribute to binding affinity through both specific interactions with PKC and less specific interactions with the membrane. For each high-affinity ligand, several hydrophobic groups of the ligand are close to the hydrophobic residues of PKC, including Pro11, Leu20, and Leu24. Furthermore, nonspecific hydrophobic interactions with the membrane are also of great importance to achieve high affinity for a PKC ligand. For example, phorbol-13-acetate and PDBu have the same hydrogen-bonding network with PKC and similar hydrophobic contacts with PKC, but PDBu is 40 000 times more potent than phorbol-13-acetate, and this disparity is attributed to the greater hydrophobicity of PDBu.

Analysis by Site-Directed Mutagenesis. Analysis by site-directed mutagenesis can provide direct experimental evidence for elements in the C1 domain contributing to PKC−ligand binding. We have therefore made single mutations for several important residues around the binding sites and measured the binding affinities of these mutants to the four classes of PKC ligands in

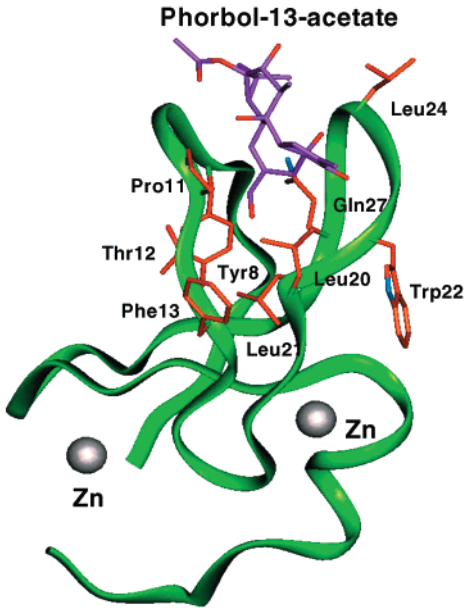

Figure 6. Mutated residues in PKCδ C1b analyzed in this study and their location in the structure of phorbol-13-acetate in complex with PKCδ C1b.

our current study. The mutated residues are shown in Figure 6, and the results are summarized in Table 1.

A number of mutations such as Leu21 → Gly, Leu24 → Gly, Gln27 → Gly, and Gln27 → Trp led to a complete loss of binding to PDBu, the reference ligand used in our binding studies. Leu21 forms a hydrophobic cluster with a number of other hydrophobic residues and may play a crucial role in determining the structure of the PKC C1b domain. Therefore, we predicted that mutation Leu21 → Gly may have significantly disrupted the binding site conformation of the PKC C1b domain. Leu24 is a hydrophobic residue that is involved in hydrophobic interactions with PKC ligands, as indicated both by the X-ray structure of PKC C1b in complex with phorbol-13-acetate and by our predicted complex structures of PKC C1b with PKC ligands. However, if Leu24 contributes solely to the hydrophobic interactions with PKC, mutation Leu24 → Gly should only result in a significant reduction in binding but not in complete abolishment of its ability to bind PDBu. Therefore, we predicted that the Leu24 → Gly mutation should alter the preferred loop conformation. The Gln27 → Gly mutation led to a total loss of binding to PDBu. From the X-ray structure, Gln27 plays an important role in determining the conformation of the binding site through formation of three hydrogen bonds with the backbones of two residues. Therefore, we predicted that mutation Gln27 → Gly may have significantly disrupted the conformation of the binding site. Mutation of Gln27 to Trp also abolishes the binding to PDBu presumably because Trp occupies a large volume in the binding site and thus prevents effective interactions with PKC ligands. It is of interest to note that mutation Gln27 → Val partially restores the binding to PDBu, but the mutant is 40-fold less potent than the wild-type PKC C1b.

Among the four classes of PKC ligands examined here, ILV appears to be the ligand most sensitive to structural perturbations in PKC and consistently shows the largest reduction in binding affinity for each mutant, whereas ingenol-3-benzoate shows the smallest reduction in its binding affinity for each mutant. Among mutations leading to quantitative reductions in binding affinity for PKC ligands, the Pro11 → Gly mutation has the largest effect. The relative reduction in binding affinity is 3500-, 600-, 150-, and 83-fold for ILV, PDBu, thymeleatoxin, and ingenol-3-benzoate, respectively. Pro11 is located on the binding loop formed between residues 8 and 13, and because of its cyclized structure, Pro11 restricts the loop conformation. Mutation of Pro11 to Gly results in a loss in this conformational restriction and may have resulted in a significant change in the loop conformation. Furthermore, the X-ray structure of PKCδ C1b in complex with phorbol-13-acetate and our predicted binding models for the other four high-affinity ligands showed that Pro11 has close contacts with hydrophobic groups in the PKC ligands and is thus important for hydrophobic interactions. The significant reduction in binding affinity of Pro11 → Gly probably reflects the combined effect of these two aspects. The side chain of Tyr8 is part of a hydrophobic core on the bottom of the ligand binding-site. Mutation of Tyr8 should result in a perturbation in the binding site conformation, affecting the binding affinity to ligands. Indeed, mutation Tyr8 → Gly reduces the binding affinity by 330-, 52-, 32-, and 24-fold for ILV, PDBu, thymeleatoxin, and ingenol-3-benzoate, respectively. In the X-ray structure and our predicted complex structures, the backbone amide group of Thr12 forms a hydrogen bond to each ligand. Although the side chain of Thr12 is partially exposed to solvent and does not directly interact with ligands, mutation Thr12 → Gly may somewhat perturb the binding site conformation, especially with respect to the backbone conformation of residue 12 itself. However, this perturbation should be relatively small because mutation Thr12 → Gly only has a moderate effect on the binding affinity of these ligands. Phe13 is a hydrophobic residue, but its side chain is exposed to solvent. Phe13 does not directly participate in ligand−PKC interactions, as shown by both the X-ray structure and the predicted complex structures. Consistent with the predicted complex structures, mutation Phe13 → Gly has only a minimal effect on the binding of these ligands to PKC. Similar to Phe13, Leu20 also is a hydrophobic residue and its side chain is exposed to solvent. Different from Phe13, Leu20 was found to directly interact with these PKC ligands based on our predicted complex structures. For example, on the basis of the predicted complex structure of ILV to PKC, the *N*-methyl group is close to the side chain of Leu20, contributing to the overall hydrophobic interactions between ILV and PKC. Therefore, mutation Leu20 → Gly has a much bigger effect on the binding affinity of these ligands than does Phe13 → Gly. On average, mutation Leu20 → Gly produced a 15-fold reduction compared to the wild-type PKC. It is of note that ILV has a 33-fold reduction in its binding affinity. Three mutations were made for Gln27. Of these, mutation Gln27 → Gly or Gln27 → Trp resulted in mutants that had no measurable binding to PDBu. However, mutation Gln27 → Val restored partial binding affinity to PDBu (a 40-fold reduction). This mutant also has a reduced binding affinity to ILV, thymeleatoxin, and ingenol-3-benzoate by 552-, 17-, and 11-fold, respec-

Table 1. Analysis by Site-Directed Mutagenesis of the Binding of PKC Ligands to PKCδ C1b

	PDBu		ILV		ingenol-3-benzoate		thymeleatoxin	
	K_i[a] (nM)	ratio[c]	K_i[a] (nM)	ratio[c]	K_i (nM)	ratio[c]	K_i (nM)	ratio[c]
wild-type	0.351 ± 0.054		2.01 ± 0.17		0.13 ± 0.03		2.71 ± 0.59	
T8G	18.4 ± 1.4	52	658 ± 29	327	3.14 ± 0.12	24	86.6 ± 7.7	32
P11G	210 ± 15	598	7080 ±770	3520	10.8 ± 1.4	83	417 ± 120	154
T12 G	1.24 ± 0.23	3.5	25.3 ± 2.5	13	0.72 ± 0.12	5.5	19.1 ± 1.4	7.1
F13G	0.82 ± 0.13	2.3	10.9 ± 0.8	5.4	0.15 ± 0.02	1.2	7.8 ± 1.3	2.9
L20G	6.59 ±0.3	15	66.2 ± 6.2	33	1.08 ± 0.20	8.3	11.27 ± 0.65	4.2
L21G	no binding	>1000	*b*		*b*		*b*	
W22G	25.0	31	*b*		*b*		*b*	
L24 G	no binding	>1000	*b*		*b*		*b*	
Q27G	no binding	>1000	*b*		*b*		*b*	
Q27V	14.2 ± 1.5	40	1100 ± 140	552	1.41 ± 0.07	11	47.1 ± 4.3	17.4
Q27Q	no binding	>1000	*b*		*b*		*b*	

[a] Data taken from ref 19. [b] Not Determined. If the mutant does not have a significant binding to the reference ligand [^{3}H]PDBu, the binding affinity of the mutant to nonradioactive ligands cannot be determined. [c] Ratio is the calculated binding affinity of the ligand for the mutant to that of the wild-type.

tively. On the basis of the X-ray structure and our predicted complex structures, Gln27 does not directly interact with ligands. However, the side chain of Gln27 forms a total of three hydrogen bonds, two with the backbone of Tyr8 and one with the backbone carbonyl of Gly23. These hydrogen bonds may play an important role in maintaining the optimal binding site conformation for interactions with ligands. Mutation Gln27 → Gly may have significantly distorted the binding site conformation. Mutation Gln27 → Trp may simply fill in the binding pocket and make the binding site inaccessible to ligands. In summary, our mutagenic analyses provided quantitative assessment and new insights into the binding of PKC to its ligands. The results obtained from site-directed mutagenetic analysis are consistent with the X-ray structure and our predicted binding models for the ligands examined here.

Investigation of the Structural Perturbations Caused by Mutation through Molecular Dynamics Simulation. In theory, each mutation can affect ligand binding to the receptor through alteration of the direct interactions between the ligand and the receptor, or through an overall change in conformation of the binding site, or through both mechanisms. As an extreme example of the second mechanism, some mutations may make the protein unable to fold properly. To gain more structural insights into the binding of PKC to its ligands, we have performed extensive molecular dynamics simulations on the wild-type of PKCδ C1b and its 11 mutants to investigate the structural perturbations caused by each mutation. We made an assumption that each mutant is still able to fold and assumes the overall fold of the wild-type PKC. To characterize the binding-site conformation, we analyzed the backbone torsion angles for residues 7−13 and 20−28, which form the binding site for the wild-type protein and mutants during MD simulations. The backbone average torsion ϕ and ψ angle values for these residues as well as their fluctuations are provided in Table 2.

In the X-ray structure of PKCδ C1b, Leu21 is located at the bottom of the binding site and forms a hydrophobic core. Experimentally, mutation Leu21 → Gly completely abolished the binding of PKC to PDBu, and yet this residue does not have strong hydrogen bonding or hydrophobic interactions with PKC ligands. We predicted that the complete loss by this mutant of its ability to bind to PDBu probably reflects a significant conformational change of the binding site upon mutation. Our simulation results support this prediction. As can be seen in Table 2, mutation Leu21 → Gly alters the average ϕ and ψ values for residue 21 by 66° and 45°, respectively. The mutation also alters the average ψ value for Leu20 by 94°. Since Leu21 and Tyr8 form a hydrogen bond through their backbones, this mutation also led to a change in the average ψ value for Tyr8 by as much as 57°. Thus, mutation Leu21 → Gly profoundly affects the conformations of both loops that form the binding site, and this conformational change makes the protein unable to bind to PDBu.

Mutation Leu24 → Gly completely abolished the ability of PKC to bind to ligands. On the basis of the X-ray structure of PKCδ C1b in complex with phorbol-13-acetate and our predicted binding modes of several other PKC ligands in the present study, Leu24 makes direct contacts with ligands and contributes to binding through hydrophobic interactions. Our previous analysis showed that the hydrophobic contribution by Leu24 cannot fully account for the total loss in the binding ability of PKC to ligands. We predicted that Leu24 → Gly must cause a significant binding-site conformational change. Our simulation results support this prediction. As can be seen from Table 2, mutation Leu24 → Gly alters the average ψ value for Gly23 by 45° and the average ϕ value for residue 24 by 30°. Furthermore, the fluctuations of these two torsion angles in the mutant are much larger than those in the wild-type PKC, suggesting that the loop formed by residues 20−28 becomes more flexible upon mutation. On the basis of the X-ray structure of PKCδ C1b in complex with phorbol-13-acetate and the predicted binding models for several other ligands in the present study, Gly23 forms two hydrogen bonds with ligands. The change of backbone conformation of Gly23 upon mutation greatly affects the ability of Gly23 to form optimal hydrogen bonds with ligands.

In the X-ray structure of PKCδ C1b, Gln27 forms three hydrogen bonds through its side chain with the backbone of Tyr8 and Gly23, thus playing an important role in maintaining the binding-site conformation. Experimentally, mutation Gln27 → Gly abolished the binding ability of PKC to PDBu. Although Gln27 has weak hydrogen-bonding interactions with phorbol-13-acetate in the X-ray structure, we predicted that the complete loss by this mutant in its ability to bind to

Table 2. Average and Fluctuation Values of the Backbone Angles for Residues 7−13 and 20−28 for Wild Type and Mutants during MD Simulations[a]

(a) φ Angles

	Asn 7	Tyr 8	Met 9	Ser 10	Pro 11	Thr 12	Gly 13	Leu 20
wild	−113 ± 12	−117 ± 14	−101 ± 15	−82 ± 12	−64 ± 8	−119 ± 13	−108 ± 11	−73 ± 10
L21G	−117 ± 13	−94 ± 10	−104 ± 17	−85 ± 14	−68 ± 9	−126 ± 21	−108 ± 14	−94 ± 10
L24G	−113 ± 12	−116 ± 15	−94 ± 16	−89 ± 14	−65 ± 9	−117 ± 14	−91 ± 12	−82 ± 12
Q27G	−108 ± 11	−100 ± 14	−100 ± 13	−112 ± 18	−63 ± 7	−117 ± 13	−95 ± 10	−77 ± 11
Q27W	−106 ± 14	−99 ± 21	−103 ± 18	−90 ± 16	−63 ± 8	−120 ± 14	−94 ± 10	−79 ± 11
Q27V	−107 ± 12	−106 ± 24	−98 ± 12	−79 ± 12	−63 ± 8	−122 ± 12	−110 ± 11	−69 ± 9
P11G	−115 ± 12	−119 ± 15	−99 ± 19	−93 ± 17	**−144 ± 43**	−110 ± 17	−94 ± 10	−84 ± 12
L20G	−105 ± 11	−119 ± 15	−95 ± 14	−87 ± 15	−65 ± 8	−117 ± 14	−108 ± 11	−80 ± 14
W22G	−113 ± 13	−106 ± 14	−102 ± 14	−84 ± 13	−64 ± 8	−118 ± 13	−105 ± 11	−79 ±11
Y8G	−88 ± 11	−108 ± 27	−95 ± 17	−91 ± 18	−67 ± 8	−122 ± 15	−99 ± 11	−83 ± 12
T12G	−103 ± 13	−91 ± 11	−89 ± 13	−99 ± 15	−76 ± 9	**−153 ± 22**	−111 ± 20	−82 ± 12
F13G	−113 ± 13	−121 ± 13	−96 ± 14	−85 ± 14	−65 ± 8	−117 ± 16	−106 ± 14	−78 ± 12

	Leu 21	Trp 22	Gly 23	Leu 24	Val 25	Lys 26	Gln 27	Gly 28
wild	−87 ± 9	−110 ± 21	149 ± 21	−97 ± 18	−96 ± 14	63 ± 11	−78 ± 13	−148 ± 21
L21G	**−153 ± 33**	−97 ± 15	151 ± 27	−91 ± 13	−105 ±15	53 ± 13	−78 ± 11	−147 ± 18
L24G	−90 ± 10	−96 ± 17	140 ± 27	**−127 ± 58**	−105 ±15	57 ± 12	−79 ± 12	−149 ± 18
Q27G	−78 ± 9	**−73 ± 10**	**−177 ± 14**	−97 ± 11	−80 ±9	52 ± 9	−95 ± 17	176 ± 13
Q27W	−83 ± 9	−126 ± 16	173 ± 16	−97 ± 15	−104 ± 16	67 ± 9	−83 ± 13	−153 ± 18
Q27V	−81 ± 8	−82 ± 13	141 ± 20	−96 ± 13	−111 ± 14	55 ± 9	−84 ± 10	−167 ± 14
P11G	−87 ± 9	−92 ± 18	144 ± 22	−94 ± 15	−113 ± 15	57 ± 11	−78 ± 11	−152 ± 16
L20G	−79 ± 8	−129 ± 16	−170 ± 16	−89 ± 19	−93 ± 12	**−108 ± 17**	−84 ± 14	−172 ± 13
W22G	−89 ± 10	−160 ± 33	138 ± 22	−94 ± 16	−108 ± 16	54 ± 12	−77 ± 11	−162 ± 16
Y8G	−82 ± 9	−94 ± 17	153 ± 21	−91 ± 12	−97 ± 13	**−86 ± 9**	−95 ± 15	−146 ± 26
T12G	−89 ± 12	−103 ± 16	148 ± 18	−96 ± 17	−123 ± 14	50 ± 12	−78 ± 10	162 ± 16
F13G	−82 ± 8	−126 ± 16	−164 ± 14	−87 ± 17	−93 ± 12	−108 ± 17	−81 ± 12	160 ± 15

(b) ψ Angles

	Asn 7	Tyr 8	Met 9	Ser 10	Pro 11	Thr 12	Gly 13	Leu 20
wild	143 ± 13	153 ± 17	−51 ± 11	154 ± 11	115 ± 13	133 ± 9	158 ± 9	140 ± 7
L21G	143 ± 11	**96 ± 17**	−48 ± 12	152 ± 15	103 ± 27	132 ± 14	154 ± 17	**−134 ± 27**
L24G	141 ± 15	157 ± 14	−56 ± 13	154 ± 14	125 ± 19	140 ± 12	152 ± 8	149 ± 9
Q27G	121 ± 13	160 ± 10	−48 ± 13	162 ± 9	121 ± 14	143 ± 8	156 ± 8	151 ± 9
Q27W	123 ± 19	148 ± 17	−58 ± 12	161 ± 10	115 ± 13	138 ± 9	152 ± 8	145 ± 8
Q27V	114 ± 28	142 ± 14	−43 ± 12	147 ± 11	113 ± 12	139 ± 9	160 ± 8	146 ± 7
P11G	144 ± 14	165 ± 17	−63 ± 14	**−102 ± 45**	102 ± 18	136 ± 9	154 ± 8	147 ± 8
L20G	146 ± 15	149 ± 18	−53 ± 16	160 ± 10	119 ± 16	136 ± 9	154 ± 8	144 ± 8
W22G	132 ± 14	146 ± 17	−51 ± 13	150 ± 12	111 ± 12	133 ± 9	155 ± 9	135 ± 8
Y8G	127 ± 21	117 ± 32	−53 ± 15	152 ± 13	126 ± 20	141 ± 12	156 ± 8	145 ± 8
T12G	117 ± 13	122 ± 20	−47 ± 12	**125 ± 15**	**168 ± 14**	−172 ± 18	154 ± 11	148 ± 11
F13G	150 ± 13	158 ± 14	−55 ± 13	156 ± 11	110 ± 15	139 ± 9	155 ± 10	143 ± 8

	Leu 21	Trp 22	Gly 23	Leu 24	Val 25	Lys 26	Gln 27	Gly 28
wild	93 ± 15	155 ± 11	160 ± 19	−64 ± 16	118 ± 13	80 ± 19	−57 ± 13	154 ± 28
L21G	**138 ± 20**	150 ± 25	178 ± 15	−64 ± 14	160 ± 12	58 ± 12	−50 ± 15	174 ± 13
L24G	94 ± 18	172 ± 30	**−155 ± 53**	−79 ± 18	153 ± 13	64 ± 12	−53 ± 15	169 ± 19
Q27G	**−175 ± 14**	**−39 ± 13**	−154 ± 12	−66 ± 12	119 ± 9	55 ± 12	**−14 ± 21**	177 ± 12
Q27W	83 ± 15	166 ± 14	−166 ± 21	−76 ± 16	120 ± 14	107 ± 23	**55 ± 13**	159 ± 17
Q27V	97 ± 11	146 ± 13	−179 ± 15	−69 ± 14	156 ± 10	61 ± 12	−31 ± 10	175 ± 13
P11G	87 ± 16	162 ± 16	177 ± 16	−71 ± 14	153 ± 12	62 ± 11	−50 ± 14	171 ± 17
L20G	92 ± 14	160 ± 11	−167 ± 25	−65 ± 13	**−66 ± 13**	153 ± 19	−61 ± 12	173 ± 13
W22G	114 ± 26	173 ± 19	−160 ± 22	−79 ± 19	156 ± 13	61 ± 13	−49 ± 12	179 ±14
Y8G	116 ± 19	138 ± 19	−178 ± 18	−84 ± 18	**−57 ± 8**	101 ± 18	−60 ± 20	−171 ± 14
T12G	91 ± 19	155 ± 17	−174 ± 17	−71 ± 15	159 ± 12	57 ± 12	−35 ± 15	−180 ± 12
F13G	94 ± 12	161 ± 11	−168 ± 22	−65 ± 14	−69 ± 13	159 ± 15	−55 ± 13	−175 ± 12

[a] Significant changes in the backbone angles are highlighted in bold.

PDBu is primarily due to a significant conformational change of the binding site. As can be seen from Table 2, our simulation results support this prediction. Mutation Gln27 → Gly alters the average ψ value for Leu21 by 88° and the average ψ value for residue 27 by 43°. On the basis of the X-ray structure and our predicted binding models for PKC ligands, the backbone conformation of Leu21 is important for binding through formation of a strong hydrogen bond with each ligand. Thus, mutation Gln27 → Gly significantly affects the ability of Leu21 to form a strong hydrogen bond with ligands by altering the backbone conformation of Leu21. Our mutational analysis showed that mutation Gln27 → Val results in a reduced but significant binding to PKC ligands. We predicted that this mutation may cause some conformational change to the binding site but should be significantly less than that observed for the Gln27 → Gly mutation. Indeed, our simulation results showed that no significant conformational alterations were found for this mutant. Mutation Gln27 → Trp also completely abolished the binding of PKC to its ligands. Our simulation results showed that mutation Gln27 → Trp changed the average ψ value for residue 27 by 68°, suggesting that the complete loss in binding ability of this mutant to ligands is at least in part due to the conformational change upon mutation.

Because of the large size of Trp, mutation Gln27 → Trp also blocks the accessibility of the binding site to ligands, as evident from the 3D structure of this mutant.

Mutation Pro11 → Gly significantly reduces the binding of PKC to ligands. On the basis of the X-ray structure of PKCδ C1b in complex with phorbol-13-acetate and our predicted binding models for several other PKC ligands, Pro11 makes direct contacts with ligands and thus contributes to ligand binding through hydrophobic interactions. Since Pro11 has a fused, constrained five-membered ring, we also predicted that the presence of Pro at this position plays a crucial role in maintaining the optimal binding-site conformation. Our simulation results confirm our prediction. As can be seen, mutation Pro11 → Gly alters the average ψ value for Ser10 by 104° and the average ϕ value for residue 11 by 80°. Furthermore, the fluctuations of these two torsion angles in the mutant are much larger than those in the wild-type PKC, suggesting that the loop formed by residues 7−13 becomes much more flexible upon mutation.

Mutation Leu20 → Gly significantly reduced the binding affinity to ligands. On the basis of the X-ray structure and our predicted binding models for PKC ligands, Leu20 contributes to the hydrophobic interaction. It is interesting to note that our simulation results showed that although the side chain of Leu20 is located outside the binding site, mutation Leu20 → Gly significantly affects the backbone conformations of Val25 and Lys26. Therefore, the change in binding site conformation may also contribute, along with the hydrophobic interaction, to the reduction in binding affinity for each ligand.

Trp22 is located outside the binding site. Its contribution to protein−ligand binding was thought to be mainly through the hydrophobic interaction with ligands and possibly with the membrane. Our simulation results showed that indeed no significant conformational change was observed except for the backbone ϕ value of residue 22. However, since the backbone of Trp22 was not directly involved with protein−ligand interactions, this conformational change should not affect significantly the binding of PKC to its ligands.

Tyr8 is located at the bottom of the binding site, but its side chain is partially exposed to solvent. On the basis of the X-ray structure and our predicted binding models, Tyr8 is not directly involved in protein−ligand interactions. However, mutagenic analysis showed that Tyr8 → Gly significantly reduced the binding of PKC to its ligands, ranging from 327-fold for ILV to 24-fold for ingenol-3-benzoate. Our simulation results showed that mutation Tyr8 → Gly significantly changes the backbone conformation of Val25 and Lys26. Furthermore, the hydrogen bond formed between the backbones of residue 8 and Gln27 observed in the X-ray structure of PKCδ C1b is now replaced by a hydrogen bond between the backbones of residue 8 and Val25. The formation of this new hydrogen bond brings the two loops closer at one end of the binding site, making the binding pocket smaller, which may explain the significantly reduced binding affinity of this mutant to each ligand compared to wild-type PKC.

Although the side chain of Thr12 does not have direct interactions with ligands, its backbone amide group forms a strong hydrogen bond with ligands. Mutation analysis showed that mutation Thr12 → Gly results in a marginally reduced binding affinity for each ligand, ranging from 3.5- to 12.6-fold. Our simulation results showed that the Thr12 → Gly mutation affects the backbone torsion ψ angle of Pro11 and the ϕ and ψ angles of Thr12. This mutation also affects the ϕ angle of Gly28. Since Pro11 and Thr12 are directly involved in protein−ligand interactions, the change of their backbone conformations upon mutation can explain the observed reduction in binding affinity for each ligand.

Mutation analysis showed that Phe13 → Gly only slightly reduced the binding affinity to each ligand, ranging from 1.2- to 5.4-fold. Our simulation results showed that the Phe13 → Gly mutation does not significantly affect the binding-site conformation. It is interesting to note that this mutation changes the backbone conformations of Val25 and Lys26. Since Val25 and Lys26 do not have direct contacts with ligands, their conformational change should have minimal effect on the binding affinity for each ligand, consistent with the results of the mutagenesis.

In summary, our extensive simulation studies provide additional insights into the role played by each individual residue in PKC−ligand binding. Our simulation results showed that mutations of these residues have rather different effects on the structure of the protein. Some mutations affect the conformation of the protein in a global manner, some mutations produce a local conformational change, while some other mutations have only a minimal effect on the binding-site conformation. For example, mutation Leu21 → Gly causes a rather large and global conformational change, making the mutant unable to bind to PDBu. Mutation Pro11 → Gly greatly affects the loop conformation formed by residues 7−13. Mutation Phe13 → Gly has only a minimal effect on the binding site conformation. The overall effect of a mutation on the binding of PKC to its ligands is a combination of the alterations of the binding-site conformation and direct contacts.

Summary

In the current study, we sought to achieve a better understanding of the structural basis of PKC−ligand interactions through computational prediction of binding models of four classes of ligands (PDBu, ILV, ingenol-3-benzoate, and thymeleatoxin) to PKCδ C1b, through site-directed mutagenic analysis of the binding of 11 mutants to these 4 ligands, and through computational MD simulations of these 11 mutants. Taken together with the X-ray structure of phorbol-13-acetate in complex with PKCδ C1b, our predicted binding models of PDBu, ILV, ingenol-3-benzoate, and thymeleatoxin to PKC showed that the binding of these ligands to PKC is governed by a combination of several highly specific hydrogen bonds and hydrophobic interactions. In terms of hydrogen bonding, although the receptor always uses two common hydrogen bond acceptors and two common hydrogen bond donors to form hydrogen bonds with ligands, the hydrogen bond network found for each ligand is different. Furthermore, the number of hydrogen bonds between PKC and these ligands has no correlation with their binding affinity. This suggests that although hydrogen bonds are clearly

important for the specific recognition by PKC of its ligands, the importance of hydrogen bonds to ligand binding affinity needs to be further investigated. In terms of the hydrophobic interaction, the hydrophobic groups in these PKC ligands play not only a role in the hydrophobic interaction with the membrane but also a role in the interaction with a number of hydrophobic residues around the binding site, such as Pro11, Leu20, and Leu24. These interactions are shown to be important for the binding of PKC to its ligands, as confirmed by site-directed mutagenic analysis. Previous PKC pharmacophore studies often assumed that these high-affinity PKC ligands should share a set of common hydrogen bond donors and acceptors, which can overlap nicely in a three-dimensional space. Our current studies showed that previously proposed pharmacophore models for PKC ligands are partially correct.

We employed site-direct mutagenic analysis to provide a direct and quantitative assessment of the contributions of several conserved residues around the binding site to ligand binding. The mutagenic results are consistent with the X-ray structure and our predicted binding models for these ligands. Finally, we have employed conventional MD simulations to investigate the structural perturbation caused by each of these 11 mutations. Our MD simulations showed that several mutations significantly affect the binding-site conformation, while some other mutations produce only moderate change. The large alteration in the binding-site conformation caused by these mutations is at least in part responsible for the total abolishment or significant loss in binding of these mutants to these high-affinity ligands.

Acknowledgment. Access to the Origin2000 computer was provided by the Advanced Biomedical computing center, NCI-Frederick, NIH, Frederick, MD. Their support was highly appreciated. The financial support from the Department of Defense (DOD DAMP 17-93-V-3018) for the Georgetown Institute for Cognitive and Computational Sciences is greatly appreciated.

References

(1) Nishizuka, Y. The role of protein kinase C in cell surface signal transduction and tumor promotion. *Nature* **1984**, *308*, 693−698.
(2) Nishizuka, Y. Studies and perspectives of protein kinase C. *Science* **1986**, *233*, 305−312.
(3) Nishizuka, Y. The molecular heterogeneity of protein kinase C and its implications for cellular recognition. *Nature* **1988**, *334*, 661−65.
(4) Lester, D. S., Epand, R. M., Eds. *Protein kinase C, current concepts and future perspectives*; Ellis Horword, Ltd.: New York, 1992.
(5) Kazanietz, M. G.; Areces, L. B.; Bahador, A.; Mischak, H.; Goodnight, J.; Mushinski, F.; Blumberg, P. M. Characterization of ligand and substrate specificity for the calcium-dependent and calcium-independent PKC isozymes. *Mol. Pharmacol.* **1993**, *44*, 298−307.
(6) Sharkey, N. A.; Blumberg, P. M. Comparison of the activity of phorbol 12-myristate 13-acetate and the diglyceride glycerol 1-myristate 2-acetate. *Carcinogenesis* **1986**, *7*, 677−679.
(7) Blumberg, P. M. Protein kinase C as the receptor for the phorbol ester tumor promoters. Sixth Rhoads Memorial Award Lecture. *Cancer Res.* **1988**, *48*, 1−8.
(8) Burns, D. J.; Bell, R. M. Protein kinase C contains two phorbol ester binding domains. *J. Biol. Chem.* **1991**, *266*, 18330−18338.
(9) Quest, A. F. G.; Bardes, E. S. G.; Bell, R. M. A phorbol ester binding domain of protein kinase C gamma. High affinity binding to a glutathione-S-transferase/Cys2 fusion protein. *J. Biol. Chem.* **1994**, *269*, 2953−2960.
(10) Kazanietz, M. G.; Lewin, N. E.; Gao, F.; Pettit, G. R.; Blumberg, P. M. Binding of [26-^{3}H]bryostatin 1 and analogs to calcium-dependent and calcium-independent PKC isozymes. *Mol. Pharmacol.* **1994**, *46*, 374−379.
(11) Zhang, G.; Kazanietz, M. G.; Blumberg, P. M.; Hurley, J. H. Crystal structure of the cys2 activator−binding domain of protein kinase C in complex with phorbol ester. *Cell* **1995**, *81*, 917−924.
(12) Jeffrey, A. M.; Liskamp, R. M. J. Computer-assisted molecular modeling of tumor promoters: Rationale for the activity of phorbol esters, teleocidin B and aplysiatoxin. *Proc. Natl. Acad. Sci. U.S.A.* **1986**, *83*, 241−245.
(13) Wender, P. A.; Koehler, K. G.; Sharkey, N. A.; Dell'Aquila, M. L.; Blumberg, P. M. Analysis of the phorbol ester pharmacophore on protein kinase C as a guide to the rational design of new classes of analogs. *Proc. Natl. Acad. Sci. U.S.A.* **1986**, *83*, 4214−4218.
(14) Itai, A.; Kato, Y.; Tomioka, N.; Endo, Y.; Hasegawa, M.; Shudo, K.; Fujiki, H.; Sakai, S. A receptor model for tumor promoters: Rational superposition of teleocidins and phorbol esters. *Proc. Natl. Acad. Sci. U.S.A.* **1988**, *85*, 23688-2692.
(15) Wender, P. A.; Cribbs, C. M.; Koehler, K. G.; Sharkey, N. A.; Herald, C. L.; Kamano, Y.; Pettit, G. R.; Blumberg, P. M. Modeling of the bryostatins to the phorbol ester pharmacophore on protein kinase C. *Proc. Natl. Acad. Sci. U.S.A.* **1988**, *85*, 7197−7201.
(16) Nakamura, H.; Kishi, Y.; Pajares, M. A.; Rando, R. R. Structural basis of protein kinase C activation by tumor promoters. *Proc. Natl. Acad. Sci. U.S.A.* **1989**, *86*, 9672−9676.
(17) Kong, F.; Kishi, Y.; Perez-Sala, D.; Rando, R. R. The pharmacophore of debromoaplysiatoxin responsible for protein kinase C activation. *Proc. Natl. Acad. Sci. U.S.A.* **1991**, *88*, 1973−1976.
(18) Rando, R.; Kishi, Y. Structural basis of protein kinase C activation by diacylglycerols and tumor promoters. *Biochemistry* **1992**, *31*, 2211−2218.
(19) Wang, S.; Liu, M.; Lewin, N. E.; Lorenzo, P. S.; Bhattacharrya, D.; Qiao, L.; Kozikowski, A. P.; Blumberg, P. M. Probing the binding of indolactam-V to protein kinase C through site-directed mutagenesis and computational docking simulations. *J. Med. Chem.* **1999**, *42*, 3436−3446.
(20) Pak, Y.; Wang, S. Folding of a 16-residue helical peptide using molecular dynamics simulation with Tsallis effective potential. *J. Chem. Phys.* **1999**, *111*, 4359−4361.
(21) Pak, Y.; Wang, S. Application of a molecular dynamics simulation method with a generalized effective potential to the flexible molecular docking problems. *J. Phys. Chem. B* **2000**, *104*, 354−359.
(22) Tsallis, C. Possible generalization of Boltzmann−Gibbs statistics. *J. Stat. Phys.* **1988**, *52*, 479−487.
(23) Curado, E. M. F.; Tsallis, C. Generalized statistical mechanics: connection with thermodynamics. *J. Phys. A* **1991**, *24*, L69.
(24) Andricioaei, I.; Straub, J. E. Generalized simulated annealing algorithms using Tsallis statistics: Application to conformational optimization of a tetrapeptide. *Phys. Rev. E* **1996**, *53*, R3055−R3058.
(25) Andricioaei, I.; Straub, J. E. On Monte Carlo and molecular dynamics methods inspired by Tsallis statistics: Methodology, optimization, and application to atomic cluster. *J. Chem. Phys.* **1997**, *107*, 9117−9124.
(26) Brooks, B. R.; Bruccoleri, R. E.; Olafson, B. D.; States, D. J.; Swaminathan, S.; Karplus, M. CHARMM: A program for macromolecular energy, minimization, and dynamics calculations. *J. Comput. Chem.* **1983**, *4*, 187−217.
(27) MacKerell, A. D., Jr.; Bashford, D.; Bellott, M.; Dunbrack, R. L., Jr.; Evanseck, J. D.; Field, M. J.; Fisher, S.; Gao, J.; Guo, H.; Ha, S.; Joseph-McCarthy, D.; Kuchnir, L.; Kuczera, K.; Lau, F. T. K.; Mattos, C.; Michnick, S.; Ngo, T.; Nguyen, D. T.; Prodhom, B.; Reiher, W. E., III; Roux, B.; Schlenkrich, M.; Smith, J. C.; Stote, R.; Straub, J.; Watanabe, M.; Wiorkiewicz-Kuczera, J.; Yin, D.; Karplus, M. All-atom empirical potential for molecular modeling and dynamics studies of proteins. *J. Phys. Chem. B* **1998**, *102*, 3586.
(28) QUANTA, a molecular modeling system, is supplied by Molecular Simulations, Inc., San Diego, CA.
(29) Irie, K.; Isaka, T.; Iwata, Y.; Yanai, Y.; Nakamura, Y.; Koizumi, F.; Ohigashi, H.; Wender, P.; Satomi, Y.; Nishino, H. Synthesis and biological activities of new conformationally restricted analogues of (−)-indolactam-V: Elucidation of the biologically active conformation of the tumor-promoting teleocidins. *J. Am. Chem. Soc.* **1996**, *118*, 10733−10743.
(30) Kozikowski, A. P.; Wang, S.; Ma, D.; Yao, J.; Ahmad, S.; Glazer, R. I.; Bogi, K.; Acs, P.; Modarres, S.; Blumberg, P. M. Modeling, chemistry, and biology of the benzolactam analogues of ILV. 2. Identification of the binding site of the benzolactams in the CRD2 activator-binding domain of PKC δ and discovery of an ILV analogue of improved isozyme selectivity. *J. Med. Chem.* **1997**, *40*, 1316−1326.

(31) Berendsen, H. J. C.; Postma, J. P. M.; van Gunsteren, W. F.; Di Nola, A.; Haak, J. R. Molecular dynamics with coupling to an external bath. *J. Chem. Phys.* **1984**, *81*, 3684−3690.
(32) Ryckaert, J. P.; Ciccotti, G.; Berendsen, H. J. C. Numerical integration of the Cartesian equations of motion of a system with constraints: Molecular dynamics of N-alkanes. *J. Comput. Phys.* **1977**, *23*, 327−341.
(33) Kazanietz, M. G.; Wang, S.; Milne, G. W. A.; Lewin, N. E.; Liu, H. L.; Blumberg, P. M. Residues in the second cysteine-rich region of PKC relevant to phorbol ester binding as revealed by site-directed mutagenesis. *J. Biol. Chem.* **1995**, *270*, 21852−21859.
(34) Sharma, R.; Lee, J.; Wang, S.; Milne, G. W. A.; Lewin, N. E.; Blumberg, P. M.; Marquez, V. E. Conformationally constrained analogues of diacylglycerol. Ultrapotent protein kinase C (PK-C) ligands based on a racemic 5-disubstituted tetrahydro-2-furanone. *J. Med. Chem.* **1996**, *39*, 19−28.
(35) Lee, J.; Wang, S.; Milne, G. W. A.; Sharma, R.; Lewin, N. E.; Blumberg, P. M.; Marquez, V. E. Conformationally constrained analogues of diacylglycerol. Ultrapotent protein kinase C (PK-C) ligands based on a chiral 5-(acyloxymethyl)-5-(hydroxymethyl)tetrahydro-2-furanone template. *J. Med. Chem.* **1996**, *39*, 29−35.
(36) Lee, J.; Sharma, R.; Wang, S.; Milne, G. W. A.; Lewin, N. E.; Blumberg, P. M.; Marquez, V. E. Conformationally constrained analogues of diacylglycerol. Ultrapotent protein kinase C (PK-C) ligands based on a chiral 4-disubstituted heptono-1,4-lactone template. *J. Med. Chem.* **1996**, *39*, 36−45.
(37) Wender, P. A.; DeBrabander, J.; Harran, P. G.; Jimerez, J.-M.; Koehler, M. F. T.; Lippa, B.; Park, C.-M.; Siedenbiedel, C.; Pettit, G. R. The design, computer modeling, solution structure, and biological evaluation of synthetic analogs of bryostatin 1. *Proc. Natl. Acad. Sci. U.S.A.* **1998**, *95*, 6624−6629.
(38) Wang, S.; Zaharevitz, D.; Milne, G. W. A.; Sharma, R.; Marquez, V. E.; Lewin, N. E.; Blumberg, P. M. The discovery of novel, structurally diverse PK-C agonists through computer 3D-database pharmacophore search. Molecular modeling studies. *J. Med. Chem.* **1994**, *37*, 4479−4489.
(39) Qiao, L.; Wang, S.; Lewin, N. E.; Blumberg, P. M.; Kozikowski, A. P.; Structure-based design of a novel class, high affinity protein kinase C ligands. *J. Am. Chem. Soc.* **1998**, *120*, 6629−6630.

JM000488E